Correia, DM.; Costa, CM.; Rodriguez-Hernandez, J.; Tort-Ausina, I.; Teruel Biosca, L.; Torregrosa Cabanilles, C.; Meseguer Dueñas, JM.... (2020). Effect of Ionic Liquid Content on the Crystallization Kinetics and Morphology of Semicrystalline Poly(vinylidene Fluoride)/Ionic Liquid Blends. Crystal Growth & Design. 20(8):4967-4979. https://doi.org/10.1021/acs.cgd.0c00042

Effect of Ionic Liquid Content on the Crystallization Kinetics and Morphology of Semicrystalline Poly(vinylidene fluoride)/Ionic Liquid Blends.

Daniela M. Correia[a,b], Carlos M. Costa[b]*, José-Carlos Rodríguez-Hernández[c], Isabel Tort-Ausina[c], Laura Teruel Biosca[c], Constantino Torregrosa Cabanilles[c], José M. Meseguer-Dueñas[c,d], Senentxu Lanceros-Méndez[e,f], José L. Gomez Ribelles[c,d]

[a]Centre of Chemistry, University of Trás-os-Montes e Alto Douro, 5000-801Vila Real, Portugal

[b]Centre of Physics, Universidade do Minho, 4710-057 Braga, Portugal

[c]Centre for Biomaterials and Tissue Engineering, CBIT, Universitat Politècnica de València, 46022 Valencia, Spain

[d]Biomedical Research Networking Center on Bioengineering, Biomaterials and Nanomedicine (CIBER-BBN), Valencia, Spain

[e]BCMaterials, Basque Center for Materials, Applications and Nanostructures, UPV/EHU Science Park, 48940 Leioa, Spain

[f]IKERBASQUE, Basque Foundation for Science, 48013, Bilbao, Spain

KEYWORDS: PVDF; [Emim][Cl]; electroactive phase, β-phase, crystallization kinetics

---

* **Corresponding Authors**

Carlos M. Costa (cmscosta@fisica.uminho.pt),

ABSTRACT: The crystallization kinetics of poly(vinylidene fluoride), PVDF, in blends with the ionic liquid 1-ethyl-3-methylimidazolium chloride [Emim][Cl] has been studied as a function of [Emim][Cl] content up to 40 wt%. Blends were produced by solvent casting technique from diluted solutions and solvent evaporation at a temperature higher than the melting point of PVDF followed by cooling to room temperature. Polymer phase, morphology and crystallization behavior were evaluated. When crystallizing from the molten blend it was observed that [Emim][Cl] induces nucleation of PVDF in the electroactive and highly polar β-crystalline phase while pure PVDF crystallizes in the α phase with the same thermal treatments. It is shown that PVDF crystal growth segregates an amorphous phase rich in IL molecules to the surface of the films and that the ionic liquid also remains in the spaces between the lamellae or between spherulites as demonstrated by scanning electronic microscopy (SEM) and polarizing optical microscope (POM) images. DSC results of isothermal crystallization show the dependence of equilibrium melting temperature and Avrami exponent with the [Emim][Cl] content.

1. INTRODUCTION

Smart and multifunctional materials are gaining increasing interest for applications due to their ability to change their properties through external physical stimuli such as electrical and magnetic fields [1-2]. Among the different smart material types, electroactive polymer based materials, and in particularly poly(vinylidene fluoride) (PVDF), copolymers and blends have attracted special attention due to their piezoelectric properties, leading to the generation of a mechanical deformation in response to applied electrical field and vice-versa [3]. PVDF is a semi-crystalline polymer that can crystallize in five distinct crystalline phases associated with the different PVDF chain conformations, being the β phase the one with the largest piezoelectric response [4]. Further, PVDF possess high dipole moment, high dielectric constant, good thermal and chemical stability and excellent mechanical properties [5-6]. The excellent properties of PVDF allow its applicability in different areas, ranging from sensors [7] and actuators [2, 5], to batteries [8-9] and biomedical applications [10-11], among others.

Recently, a new generation of PVDF based materials has been developed, resulting from the combination of PVDF with ionic liquids (ILs). Those represent an interesting class of smart materials, based on the structural modification induced in PVDF by the presence of the IL and the ion transport properties. Thus, bending actuators [2], magnetoionic responsive materials [12], thermochromic materials [13] and humidity sensors [14] have been recently reported.

ILs are usually salts composed entirely by organic cations and organic/inorganic anions, displaying a high ionic conductivity, high chemical and thermal stability, negligible vapor pressure and a wide electrochemical window [2, 15]. The influence of the ILs incorporation into the PVDF properties has been addressed. It has been reported that the incorporation of the IL 1-ethyl-3-methylimidazolium bis(trifluoromethylsulfonyl) imide [Emim][TFSI] into PVDF induces the formation of a miscible and conductive IL-polymer blend at the

nanometer range, decreasing the fragility of the material as a result of the IL contribution to the the rearrangements of the PVDF chain segments [6]. The influence of IL cation and anion type on the electroactive phase content, thermal and dynamic mechanical properties of PVDF was also assessed, being observed that 1-ethyl-3-methylimidazolium chloride [Emim][Cl] enhanced more significantly the β-phase content, showing also a marked nucleating effect in the crystallization process [16]. Further, the IL incorporation typically enhances the electrical conductivity of PVDF, induces a plasticizing effect, decreasing the Young Modulus and yielding stress and strains, and leads to a lower glass transition temperature of the amorphous phase [2, 16-17].

On the other hand, in spite of the number of studies on the IL-PVDF interaction, few information related to the IL influence on the PVDF crystallization kinetics has been reported, which is particularly relevant as demonstrated by the extensive studies on the effect of low-molecular weight fillers (multi-walled carbon nanotubes, MWCNTs [18], clays [19], ferrite nanoparticle [20], among others) on the crystallization behavior of PVDF. In fact, it is very important from the scientific and technological points of view to understand the mechanism by which the IL can affect the nucleation and crystal growth of PVDF and the crystal phase in which PVDF chains are packed [21].

It this sense, different IL/PVDF composites were prepared to study the effect of imidazolium IL with poly(ethylene glycol) segment on the polar β phase crystallization behavior of PVDF [22]. It was shown that the temperature of the crystallization exotherm on cooling, T_c, decreases with increasing IL content increasing at the same time the fraction of PVDF crystals in β phase.

It was also observed that 1-hexadecyl-3-methyl-imidazolium bromide ([C_{16}mim][Br]) offers dual role of nucleation and plasticization at different loading concentration in the PVDF polymer matrix [23].

Studies of the non-isothermal crystallization kinetics of the PVDF copolymer poly(vinylidene fluoride)-hexafluoropropylene (PVDF-HFP) blended with N,N-diethyl-N-(2-methacryloylethyl)-N-methylammonium bis(trifluoromethylsulfonyl) imide ([Demm][TFSI]) showed that the presence of IL actually delays the crystal growth process leading to a decrease in crystallization temperature (T_c), keeping the overall crystallinity of the samples almost unaltered [24].

The crystallization kinetics of PVDF blended with the ionic liquid (1-hexyl-3-methylimidazolium chloride, [Hmim][Cl]) was studied in [25] probing that [Hmim][Cl] promotes the formation of β-phase PVDF during the recrystallization process.

The goal of the present work is to study the crystallization in melt miscible polymer blends and, since this IL affects the nucleation and growth of PVDF crystals, to characterize by DSC the isothermal crystallization kinetics of PVDF chains from molten PVDF/[Emim][Cl] blends and correlate it with the polymer crystalline phase formed and its microstructure, providing therefore, novel insights on the relevant issue of the crystallization kinetics and morphology of PVDF/IL blends.

2. EXPERIMENTAL

2.1.Materials

Poly(vinylidene fluorde), PVDF 6020 (M_w = 670 – 700 kDa), N,N-dimethylformamide (DMF) (99.5% purity) and 1-ethyl-3-methylimidazolium chloride, [Emim][Cl] with a purity of 99% were acquired from Solvay, Merck and Iolitec, respectively.

2.2.Sample preparation

The samples were prepared following the general guidelines presented in [26]. In short, PVDF/IL films were prepared by casting from a solution in DMF. In a first stage, previous to PVDF dissolution in DMF (15/85% w/w), different IL contents ranging from 5 up to 40% (w/w) were dissolved in DMF. After this step, the polymer was added and kept under magnetic agitation during 3 hours at 25 ºC. After complete homogenization of the polymer and IL, the solution was spread on a glass plate and solvent evaporation took place at 210 °C below the IL degradation temperature (> 240 ºC) [27] in an air oven (P-Selecta). Transparent PVDF/IL films were obtained with a thickness of ~ 50 µm. In order to reduce water uptake, all samples were stored under vacuum. The samples will be identified by the IL content.

2.3.Characterization techniques

Fourier transform infrared spectroscopy (FTIR) spectra were recorded using a Spectrum 100, Perkin-Elmer, in attenuated total reflection (ATR) mode over a range of 4000 to 400 cm^{-1} with a resolution of 4 cm^{-1}. FTIR spectra were performed after 64 scans for each sample.

Differential Scanning Calorimetry (DSC) was carried out with a DSC Mettler Toledo 823e for low-temperature measurements conducted (-100 ºC to 25 ºC at 20ºC/min) in the region of the glass transition and a DSC 8000 of Perkin-Elmer for scans in the

crystallization and melting region, in both cases under flowing nitrogen (N2) atmosphere. The mass of the samples was between 5 and 10 mg. Cooling and heating thermograms were recorded between 25 and 200 ºC at a heating rate of 20 ºC/min. For isothermal crystallization experiments, samples were heated to 200 ºC for 5 min and cooled down to the crystallization temperature at the highest cooling rate at which the DSC is kept under control during the whole cooling scan: 90 ºC/min.

Optical microscopy (OM) was performed with a Nikon Eclipse E600 microscope, with polarized light, between crossed polarizers, and equipped with a Linkam THMS600 thermostatic plate refrigerated with a flow of cooling air.

The morphology of the PVDF/IL films was examined with a field emission scanning electron microscope (FESEM; ZEISS Ultra-55) at 2 kV accelerating voltage. Previously, a conductive layer of sputtered platinum was deposited on the surface of the samples.

X-ray microanalysis was performed on platinum covered sample surfaces with an energy dispersive X-ray spectrometer from Oxford Instruments. The accelerating voltage during acquisition was set to 20 kV and the exposure time was adjusted to 200 seconds for all collected EDS spectra.

Atomic force microscopy (AFM) was performed with a Multimode 8 (Bruker) operating in PeakForce nanoindentation mode in air. Maps of height, elastic modulus and adhesion were simultaneously obtained with a RTESPA-300 pyramidal silicon probe (Bruker) with a force constant of 40 N/m and a nominal resonant frequency of 300 kHz. Sapphire and polypropylene samples were used as materials of known modulus to calibrate respectively deflection sensitivity and tip radius.

3. RESULTS

3.1.Polymer phase and morphology of PVDF/IL blends

In order to study the influence of [Emim][Cl] content into the chemical characteristics of PVDF and to evaluate the influence of the different IL contents into the PVDF crystalline phase, infrared analysis was performed. Figure 1 shows the infrared spectra of PVDF/[Emim][Cl] blends with different IL contents.

Independently of the IL content, the main PVDF absorption bands are observed in the FTIR spectra: In the region of 600-400 cm^{-1} (Figure 1a) the absorption bands at 532, 489 and 410 cm^{-1} are attributed to the α phase of PVDF [28]. With increasing IL content from 5 wt% to 40 wt%, the α phase absorption bands disappears while the new absorption bands at 470 and 444 cm^{-1} are both attributed to the β phase of PVDF [28].

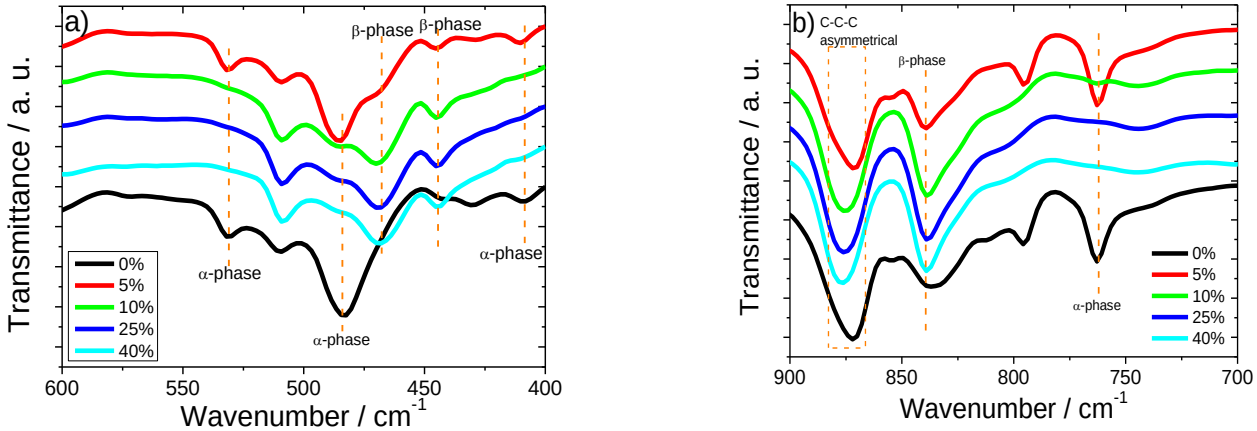

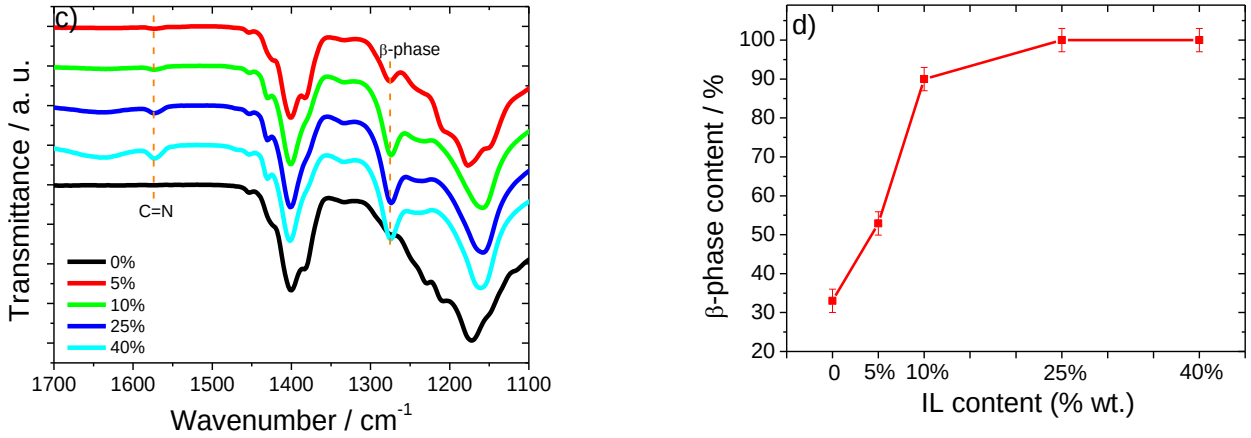

Figure 1. Infrared spectra of the PVDF/[Emim][Cl] blends from 600 to 400 cm^{-1} (a), 900-700 cm^{-1} (b) and 1300-1100 cm^{-1} (c). (d) Electroactive phase content as a function of the IL content (d).

The absorption band at approximately 878 cm^{-1} is attributed to C–C–C asymmetrical stretching vibration of PVDF (Figure 1b). This fact can be ascribed to the superposition of the spectrum of PVDF with that of [Emim][Cl], the later showing a broad bulge in this region of the spectrum. Additionally, it is observed the absence of the absorption bands at 795 and 760 cm^{-1} ascribed to the α crystalline phase. An increase in the absorption band intensity at 840 cm^{-1} assigned to the C-F stretching vibration characteristic of the all-trans planar zigzag (TTT) β phase conformation is observed [2, 4] with increasing IL content. The same occurs for the absorption band at 1275 cm^{-1} (Figure 1c), also attributed to the β phase conformation. From Figure 1c it is also observed at approximately 1600 cm^{-1} the C=N stretching vibration of the IL imidazolium ring [29].

Thus, the IL [Emim][Cl] induces the crystallization of PVDF into the electroactive β phase, as a result of the electrostatic interaction between the [Emim][Cl] with the PVDF polymer chain of > CF_2 moieties over a side of the main chain, resulting in an appropriate anion-cation pair [16, 30].

The quantification of the electroactive β phase of the PVDF/[Emim][Cl] blends was evaluated using equation (1) [4]:

$$F(\beta) = \frac{A_\beta}{\left(K_\beta / K_\alpha\right) A_\alpha + A_\beta} \quad (1)$$

where A_α and A_β are the absorbances at 766 cm^{-1} and 840 cm^{-1}, corresponding to the α and β phase, respectively, and K_α (6.1×10^4 cm^2/mol) and K_β (7.7×10^4 cm^2/mol) the corresponding absorption coefficients [4].

Figure 1d shows that the ratio of β to α crystals in the crystalline phase rapidly increases with increasing IL content in the PVDF/[Emim][Cl] blend. For neat PVDF, a β phase content of ~33% is obtained from the melt. The incorporation of 5 and 10% wt. [Emim][Cl] induces a β phase content increase to 52%, and 90%, respectively. As expected, due to the absence of the α phase absorption bands, higher IL contents (25 and 40% wt.) induces full PVDF crystallization into the electroactive β phase. These results are indicative that IL incorporation into the PVDF solution influences the PVDF crystallization process from the melt. The ion-dipole interactions between [Emim][Cl] and PVDF are stronger than the cation-anion interactions in the IL, inducing the interaction of the PVDF CF_2 groups and the CH_2 groups with the positive and negative IL charges, respectively, inducing the fully PVDF crystallization into the β phase conformation [2, 31].

[Emim][Cl] is a glass-forming liquid. Figure 2a shows the glass transition of this IL. The glass transition temperature T_g, measured as the midpoint of the heat-flow change in the transition is -95ºC. Interestingly, the thermograms of the PVDF/[Emim][Cl] blends do not show any indication of a glass transition in the temperature interval between -120 and -60ºC (Figure 2a shows the DSC thermograms measured between -120 and 0 ° C). The homogeneous mixture of two amorphous glass-forming materials yields a single glass

transition taking place at a temperature interval between those of the pure components. The glass transition temperature of the amorphous fraction of pure PVDF is -43ºC (Figure 2), that is similar to the one reported in the literature [6], nevertheless, the glass transition that appears in the blends increases with increasing IL content (Figure 2b).

The reason for this behavior is related with the crystalline form in which PVDF crystalizes in the blends. As shown above, the FTIR spectra demonstrate that pure PVDF crystallizes in the α phase while in the mixtures an increasing fraction of β phase is formed. The glass transition observed in PVDF corresponds to amorphous regions confined in the regions between crystal lamellae. From the shift of the glass transition towards higher temperatures with the addition of the IL, it can be deduced that the mobility of the amorphous regions between β phase lamellae is more restricted than that between α ones due to the different crystalline packing and stronger electrostatic interactions due to the higher polar character of the β phase. It is interesting to observe that the glass transition of [Emim][Cl] completely disappears and that it seems that there is no plasticization effect on the glass transition of PVDF segments in the amorphous phase.

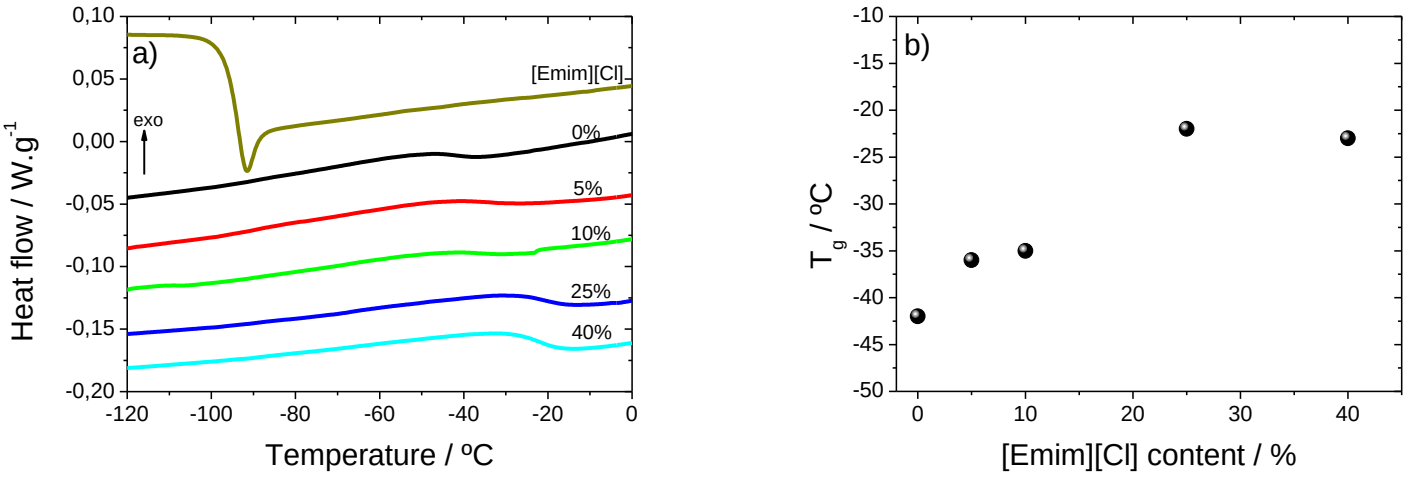

Figure 2. a) Thermogram of DSC in the region of the glass transition of the PVDF/IL samples and b) glass transition temperature as a function [Emim][Cl] content.

The microstructure of PVDF/[Emim][Cl] blends with different IL contents were analyzed by FESEM (Figure 3) and OM (Figure 4) images in samples subjected to isothermal crystallization at 150ºC. The typical PVDF spherulitic structure is shown in Figure 3a). It is to notice that some micrographs show a few inter-spherulitic pores as a result of phase separation processes and spherulitic growth kinetics, at it will be discussed further.

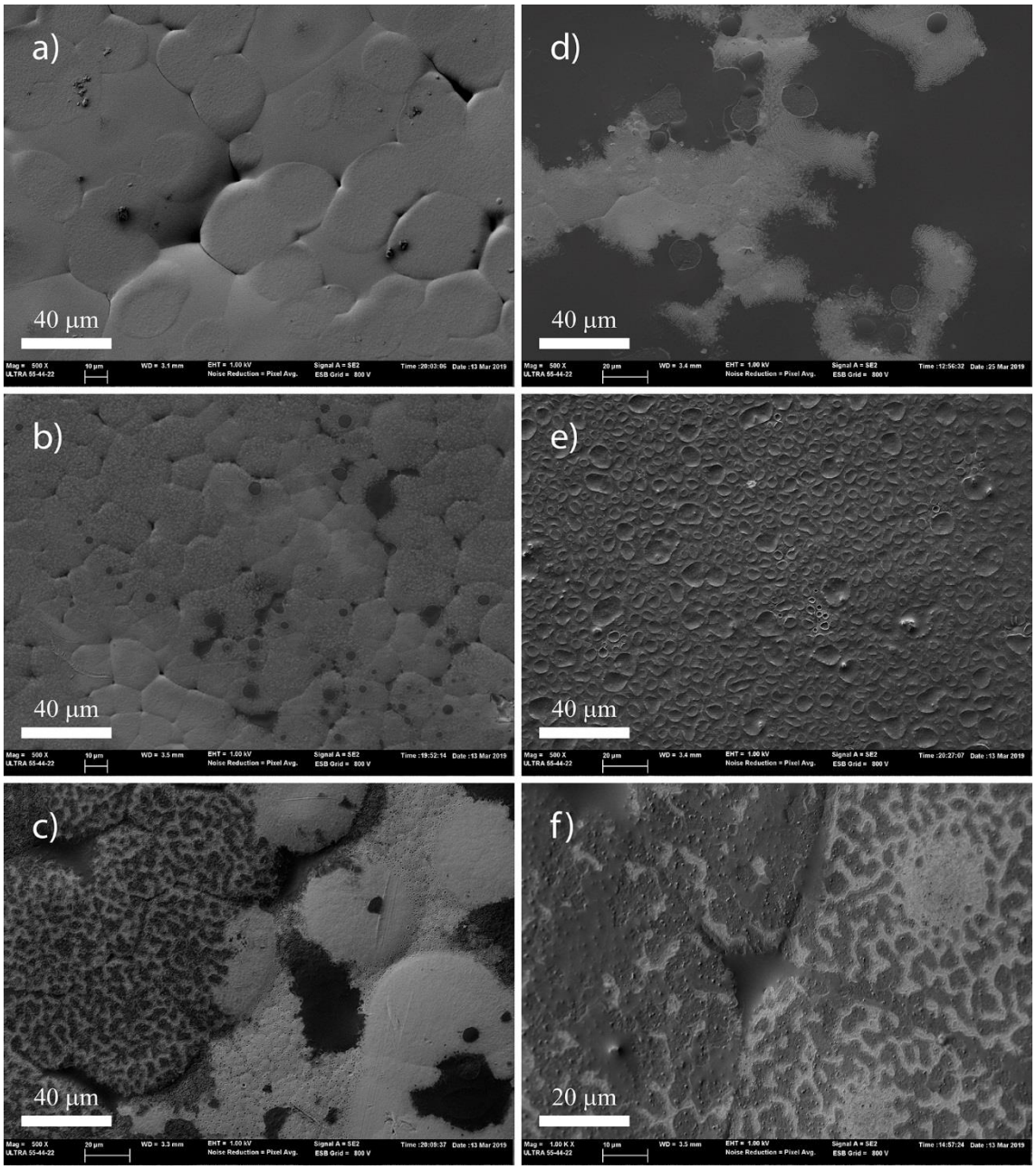

Figure 3. FESEM images at 500x of the surface of the blends crystallized at 150 ° C. (a) Net PVDF, (b) 5 wt% (c) 10wt %, (d) 25 wt%, and (e) 40 wt% IL content. (f) Magnification at 1000x for PVDF/IL samples with 10 wt% IL content.

The number and size of the spherulites are affected by the IL content in the blend. Furthermore, phase separation is clearly observed as the appearance of dark surfaces that extend over the spherulites of the PVDF, with increasing area as the content of IL in the samples increases, getting to cover completely the surface of the blend in the mixture with 40 wt% of IL, indicating that part of the IL is moved to the surface of the sample by the growth of PVDF crystals. This fact is also confirmed by the optical microscope images presented in Figure 4 in which samples containing 5 wt% and 25 wt%, crystallized at 150 °C, are observed under polarized light. The dark spots shown in the image correlate with the dark zones observed in FESEM. The partial transparency of these dark zones, which under the polarized light allows observing the PVDF spherulites below them, probes that they consist of a non-crystalline layer covering the surface. The different size of the spherulites in the samples containing different IL fractions must be ascribed to the different nucleation rate, i.e., to the different number of spherulites growing simultaneously.

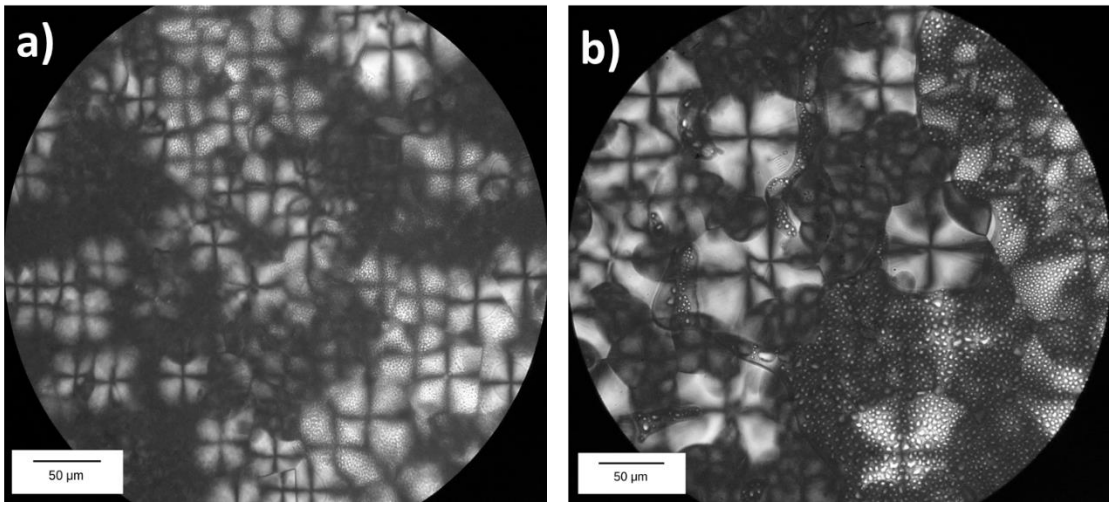

Figure 4. Optical microscopy images under polarized light of PVDF/IL samples crystallized at 150 ° C containing 5 wt% (a) or 25 wt% (b) IL content, prepared after the same protocol as the samples of Figure 3.

The distribution of [Emim][Cl] in the samples can be assessed by EDS analysis in the FESEM set up. Figure 5 shows a FESEM micrograph with the location of four points and their corresponding EDS spectra for the surface of PVDF/[Emim][Cl] blend films with 10 wt% IL content.

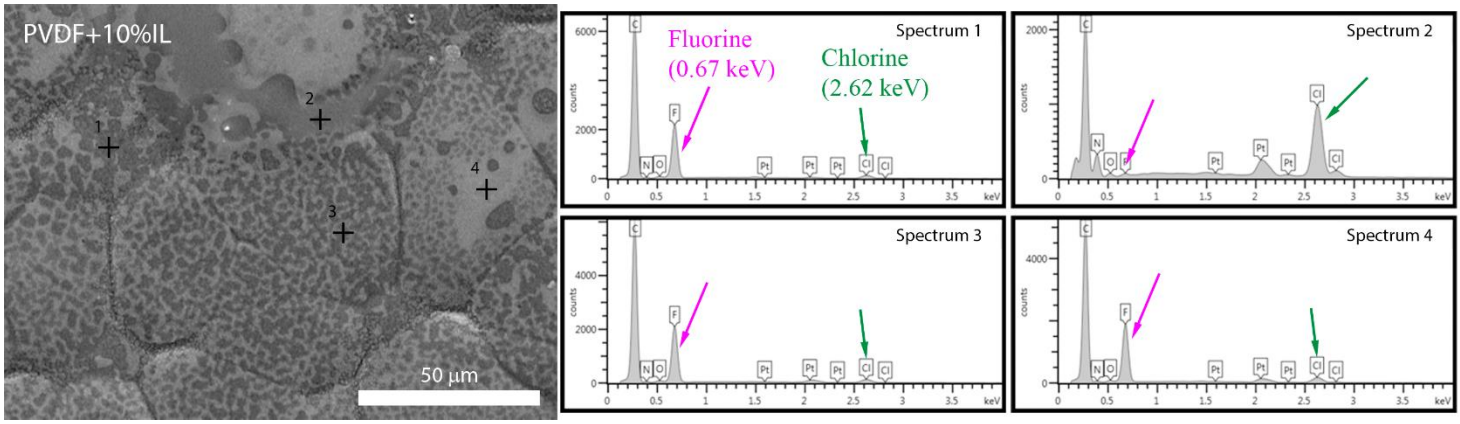

Figure 5. Elemental analysis by EDS of specific places of the surface of the PVDF/IL sample containing 10 wt% IL content, showing the fluorine (pink) and chlorine (green) peaks in dark and bright areas that appear on the surface.

It is observed an inhomogeneous distribution of IL within the PVDF polymer detected by the chlorine peaks. It is also noteworthy that as chlorine signal rises up, the fluorine peak (ascribed to the polymer) decays. Since the peaks obtained in the spectra are the result of an interaction volume of approximately 1 μm^3, small dark areas yield a low chlorine peak (the IL on the surface is low when compared to the underlying PVDF), result which is similar to those corresponding to brighter areas. However, larger dark areas show a substantial increase in the chlorine peak (and therefore a decrease in that of fluorine). This fact is also demonstrated for the other blends with different IL contents.

The cross-section of the sample was accessed using focused ion beam (FIB) technique. Figure 6a shows the FESEM image of the cut performed in the sample, the topography of the surface can also be observed, showing circular spots distributed on the surface. EDS analysis was performed in the vertical walls of the practiced trench in the different

sections indicated by points in Figure 6b. Figure 6c shows the EDS spectra demonstrating the presence of chlorine inside the sample, which indicates that part of the [Emim][Cl] remains in inter-lamellae or inter-spherulite regions.

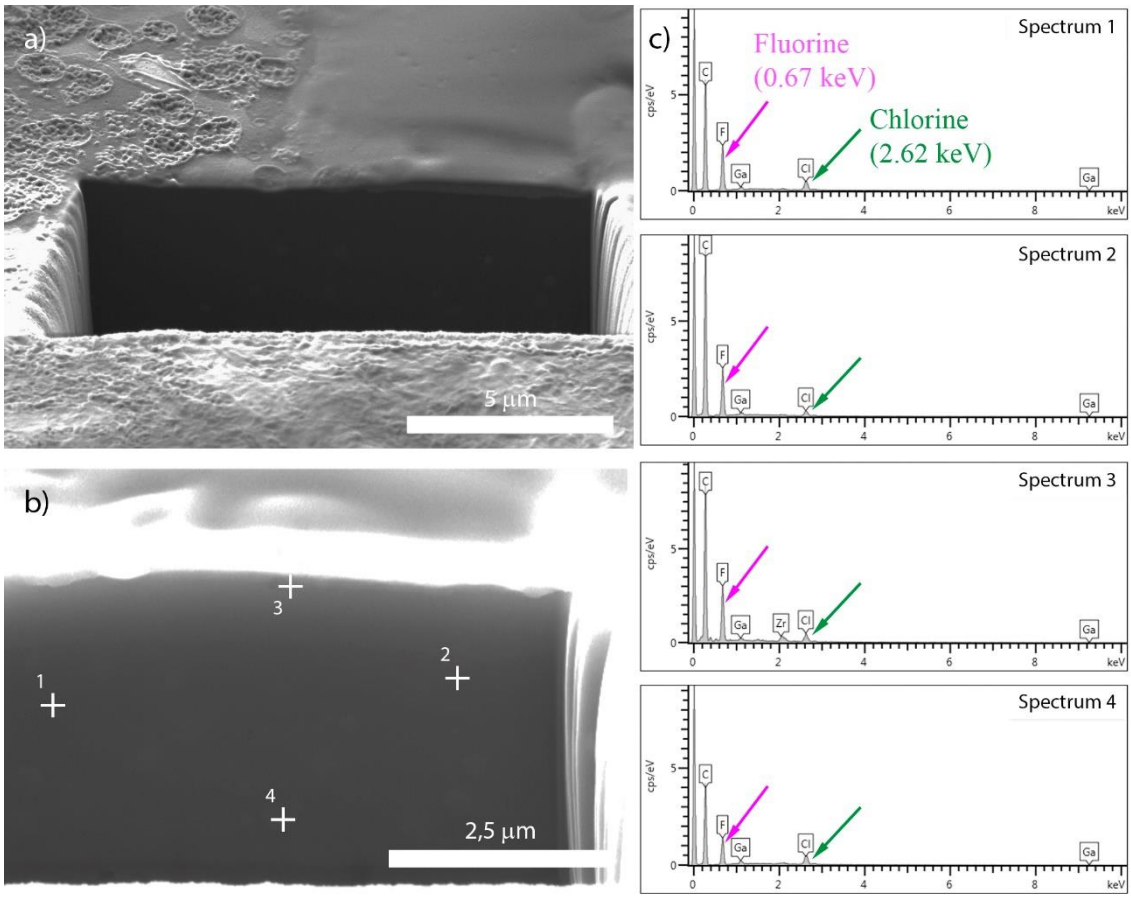

Figure 6. Micrograph obtained by means of focused ion beam (FIB) with FESEM and EDS analysis of a cross-section of a PVDF/IL sample containing 10wt% IL content. Fluorine (pink) and chlorine (green) peaks are highlighted in the EDS spectra.

In addition, morphological characterization by AFM images was performed for neat PVDF and PVDF/IL blends with 10 wt% of [Emim][Cl], as shown in Figure 7. Together with the height images, nanoindentation mapping of the sample surface was performed in which the elastic modulus and the adhesion of the tip to the surface in the retraction path were recorded. Computed surface roughness (Ra) of height AFM images ranged from 5 to 10 nm, being generally neat PVDF less rough than blends. The appearance of the thin layer that covers partially the surface of the blend is in this case clearly detected by: i)

softer regions in which the elastic modulus falls below the elastic modulus corresponding to neat PVDF; and ii) the adhesion signal. Nanoindentation was performed with a tip adequate to measure elastic modulus in the order of GPa, which are those obtained for PVDF crystals. Figure 7a shows the sharp transition along the straight line from an IL coated region to another one in which the PVDF spherulite is uncovered.

Mapping of the elastic modulus with a distance between nanoindentation points of 1 nm shows clearly the crystalline lamellae in Figure 7b at higher magnification. The oscillation of the elastic modulus (sharp peaks in Figure 7a and dark and light bands in Figure 7b) are associated with an indentation where the tip of the AFM penetrates crystalline lamellae and others where it penetrates in the amorphous inter-lamella layers. In fact, the shapes of the lamellae observed in the elastic modulus image correlate properly with features in the height image.

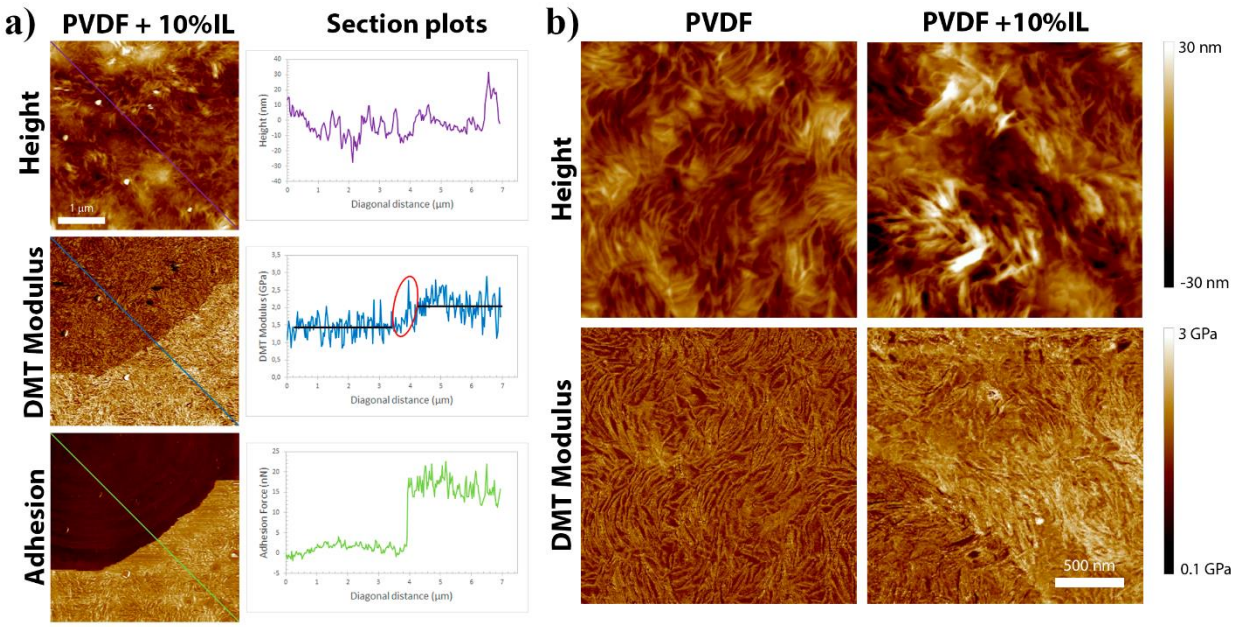

Figure 7. a) AFM pictures of height, elastic modulus and adhesion obtained by nanoindentation for PVDF/IL samples with 10 wt% IL content in the transition zone from a IL covered (left-hand side on section plots) to IL uncovered zones (right-hand side) of the surface. This transition is also highlighted in red on the DMT modulus plot; and b)

AFM pictures for height and elastic modulus for neat PVDF and PVDF/IL samples with 10 wt% IL content.

The modulus spectrum is qualitatively very similar in the neat PVDF and PVDF/IL blends (Figure 7b) although when comparing them it is necessary to highlight once again that in the case of the neat PVDF the crystallization is in α-phase, while in the PVDF/IL blends with more than 5 wt% of IL, it is in β crystalline phase.

3.2.Crystallization kinetics

Melting and crystallization in heating and cooling scans respectively were evaluated by DSC and OM images. The liquid mixture of PVDF and [Emim][Cl] is homogeneous at least with the resolution of optical microscopy. On the other hand, the crystallization temperature measured by DSC on cooling decreases as the content in IL increases (Figure 8) as predicted by thermodynamic equilibrium laws for a two-component system miscible in liquid phase and immiscible in solid phase, a phenomenon known as freezing point depression [32]. Thus, if in the liquid mixture, above the melting temperature of PVDF, the ionic liquid dissolves homogeneously in the liquid PVDF, then the crystallization on cooling and subsequent melting temperature of PVDF should decrease, as it is observed in the mixtures with [Emim][Cl]. The inset in Figure 8a) shows a schematic representation of the phase diagram of a blend which is miscible in the liquid phase but not in the solid phases. By cooling of a blend rich in PVDF, as it is the case of our blends, PVDF crystals form in equilibrium with a liquid blend which becomes richer in the IL. This equilibrium takes place at a temperature lower than that of pure PVDF. Depression of both crystallization and melting temperatures is a strong indication of the formation of PVDF crystals from a homogeneous liquid phase containing IL.

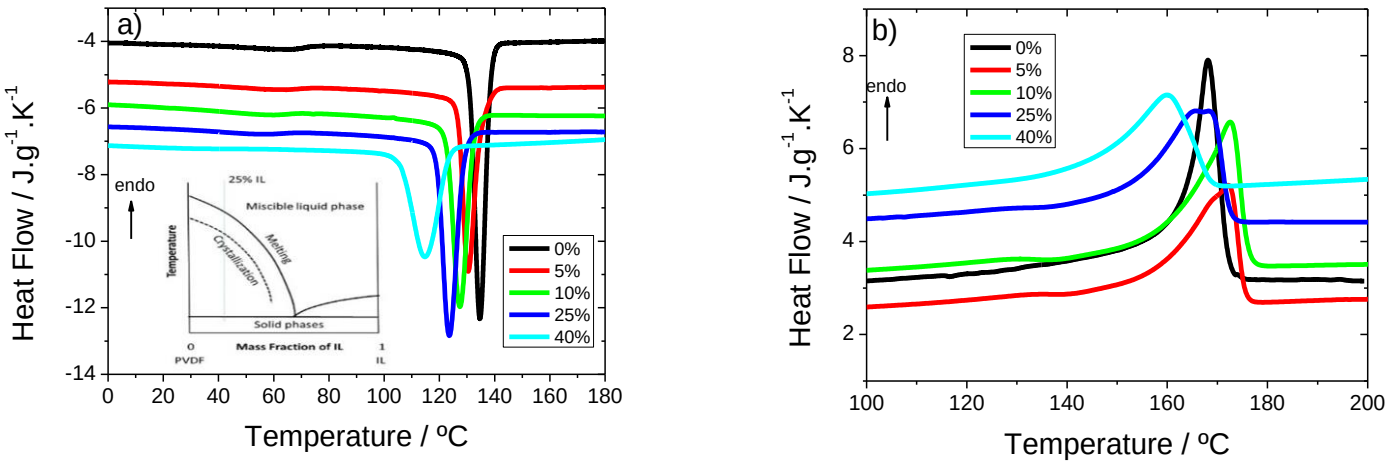

Figure 8. DSC thermograms of cooling (a) and heating (b) showing the crystallization and melting peaks, respectively, for all samples.

In the case of optical microscopy, grayscale images were obtained during cooling from 200 °C to 80 ºC at 20 °C/min and then on heating at the same rate. Figure 9 shows some representative images in the case of the PVDF/IL blend containing 25 wt% IL content. The average gray intensity and its derivative with respect to the temperature were represented, arbitrarily taking values 0 and 1 at temperatures below and above the phase transition. The maximum or minimum in the derivative of gray scale define the crystallization and melting peaks respectively.

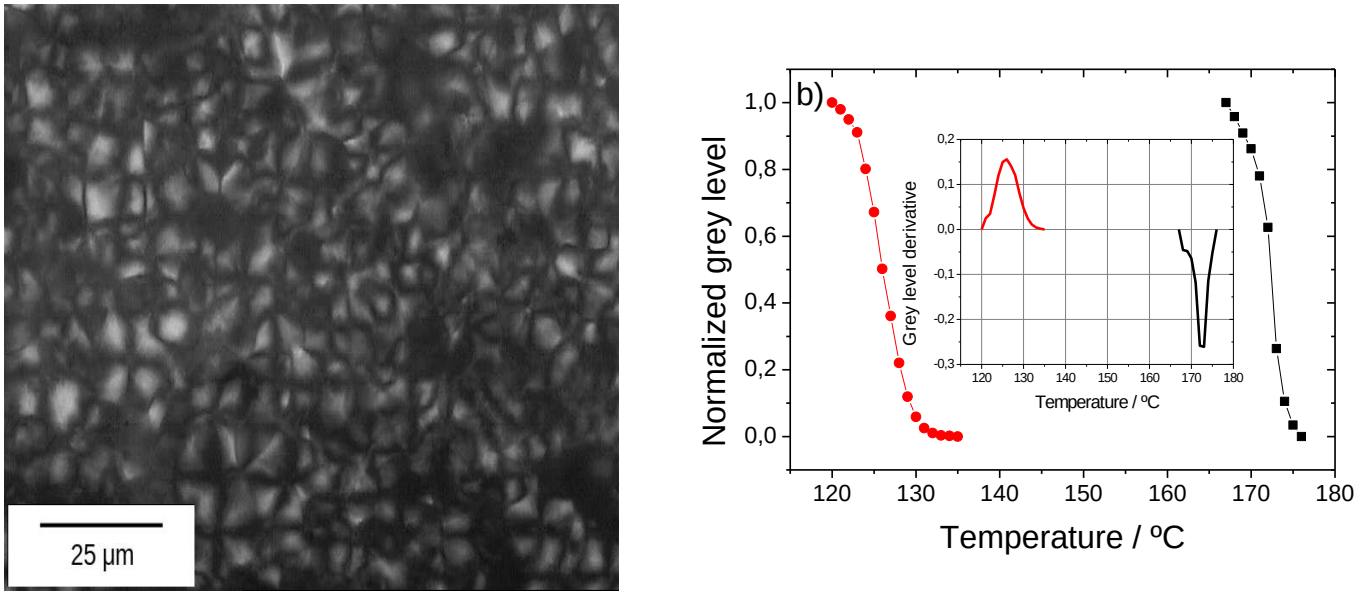

Figure 9. (a) Image captured with the polarized light optical microscope in the PVDF/[Emim][Cl] sample containing 25 wt% IL at temperatures of 120 °C during cooling scan. (b) Gray scale value and its temperature derivative as a function of temperature. The red line corresponds to cooling scan while the black line corresponds to heating ones.

Figure 10 shows the equilibrium diagram that can be determined for the crystallization and melting temperature measured by both DSC and OM at 20 °C/min. In the case of crystallization and melting temperatures measured by DSC, the maximum of the exothermic or endothermic peaks measured in the cooling and heating scans were obtained, respectively (Figure 10).

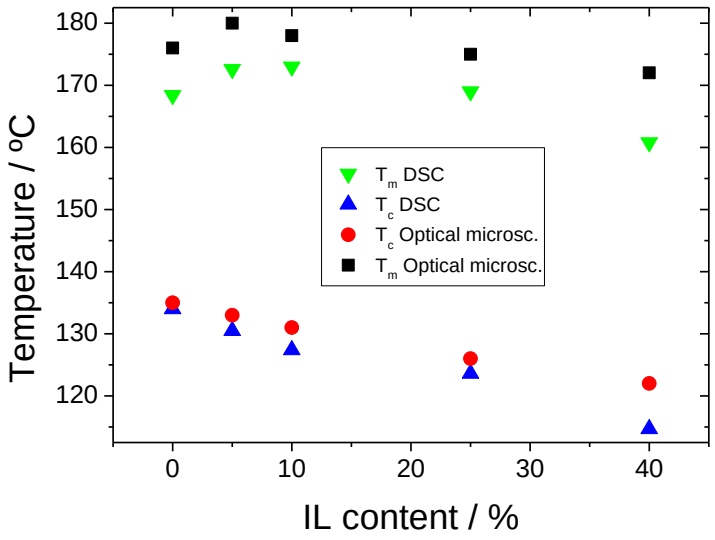

Figure 10. Phase equilibrium diagram showing melting and crystallization temperatures as a function of [Emin][Cl] content in the PVDF/IL samples.

Figure 10 shows that the crystallization and melting temperatures, T_c and T_m respectively, depend on IL content. DSC and OM measurements agree with each other in the dependence of both T_c and T_m with the IL content of the blend. The decrease of T_c with IL content, due to cryogenic descent, has been already indicated above. In the melting

temperatures, the same phenomenon appears but in this case the extrapolation of the values obtained in the blends is not coincident with the value of T_m of pure PVDF since the polymer is crystallized in the β phase in the blends while it crystallizes in the α phase in pure PVDF and the melting temperature of the β phase is higher [4].

Isothermal crystallization experiments were performed in DSC by cooling the sample from the liquid state at the maximum rate at which the DSC maintained the temperature control during the whole cooling process, 90 ºC/min. The range of crystallization temperatures was restricted to the temperature interval above the onset of the exothermal peak measured on cooling at that cooling rate thus ensuring that the whole crystallization process takes place at the programmed temperature. At the end of the isothermal stage, the melting temperature was measured by a heating scan from T_c. These heating thermograms are shown in Figure 11a) for the PVDF/IL blend with 25 wt% IL content, while some examples of the isothermal traces are shown in Figure 12.

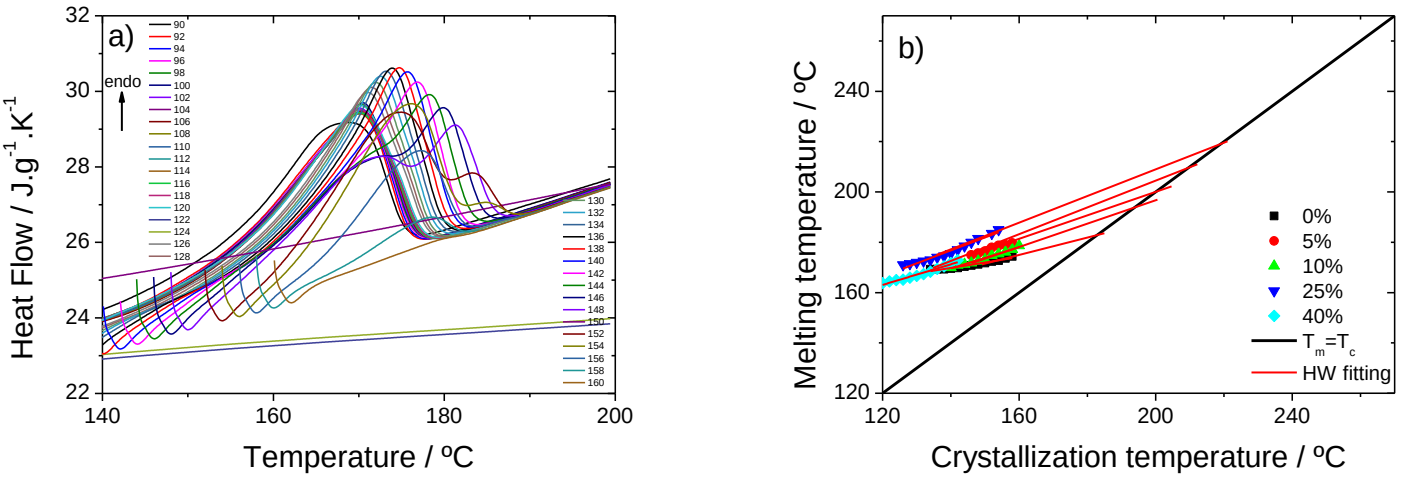

Figure 11. (a) Heating DSC thermograms measured after isothermal crystallization at different crystallization temperatures (indicated in the figure, temperatures in ºC) in the PVDF/IL samples with 25 wt% IL and (b) Hoffman-Weeks diagram.

It has been reported in the literature that the melting temperature of the β phase of PVDF in pristine PVDF is not significantly different from that of the α phase [4], while that of phase γ is of the order of 8 ºC higher when the latter is formed by isothermal crystallization at high temperature from the melt [4, 33]. It is worth noticing that in the temperature interval in which melting takes place after crystallization at the highest temperatures is too high to allow any re-crystallization during the heating scan that could make double peaks to appear.

The dependence of the melting temperature on T_c allows the Hoffman-Weeks diagram T_m vs T_c to be constructed, in which by extrapolation to $T_m = T_c$, the equilibrium melting temperature, (T_m^0), can be determined through the following equation [34]:

$$T_m = \frac{T_c}{\delta} + T_m^0\left(1 - \frac{1}{\delta}\right) \quad (2)$$

where δ is the thickening ratio.

In the heating thermograms in the range 152 ºC ≤ T_c ≤ 158 ºC, two or even three endothermic peaks appear that could be ascribed to the formation of a different crystalline phases, including the formation of γ phase. Table 1 shows the equilibrium melting temperature, (T_m^0) and thickening ratio, δ, obtained by fitting equation 1 to the data in figure 11b) for all PVDF/IL blends. The T_c interval for fitting is shown in the Table.

Table 1 - Equilibrium melting temperature (T_m^0) and thickening ratio, δ, obtained through the equation 2.

Samples	Fitting T_c interval (ºC)	T_m^0 / ºC	δ	Expected crystalline phase formed at the fitting T_c interval

0%	135÷158	178	4.6	α
5%	140÷158	195	2.4	α+β
10%	140÷158	191	2.4	α+β
25%	135÷154	245	1.5	β+γ
40%	130÷144	230	1.7	β+γ

For neat PVDF, T_m^0 is 178 ºC, which is in agreement with values reported in the literature for PVDF crystallized in the α-phase [35-36]. Also, the thickening ratio value is 4.6 due to chain mobility effects by the longer residence time at crystallization temperature [37]. For PVDF/IL blends, the extrapolation points in the Hoffman-Weeks diagram leads to somewhat higher values when compared to neat PVDF. For PVDF/IL blend with 5wt% IL, this behavior is more similar to neat PVDF as it crystallizes in the α-phase. For 10wt% IL content, the heating thermograms are very complex with up to three endothermic peaks, probably representative of regions that crystallize in two phases (α and β-phase).

It is interesting to see that when the PVDF crystallizes during the cooling scan at 20 ° C/min, the melting temperature of the PVDF/IL blend with 25 wt% IL is lower than that of PVDF/IL blends with lower IL content (5 or 10 wt%), as shown in Figure 10 and as corresponds to the equilibrium diagram. Nevertheless, after isothermal crystallization the melting temperatures are in the mixture of 25 wt% of IL significantly higher than those of the other IL contents or that of neat PVDF.

With respect to the position of the higher temperature peak in the thermograms obtained for the samples with 25% or 40% [Emim][Cl], a change of slope is observed around 135ºC in the 25% and 130ºC in the 40% one (Figure 11b): for the higher crystallization temperatures, the values in the Hoffman-Weeks diagram extrapolates to quite high values of T_{0m}, around 230 to 240ºC which have been reported as representative of β and γ phases [38], while the maxima measured in the heating thermograms after crystallization at lower temperatures extrapolate to values of T_{0m} much lower, in the range of that expected for the α phase and similar what it is found for pure PVDF and the blends containing 5% or

10% [Emim][Cl]. The values of T_m^0 listed in Table 1 for the samples containing 25% or 40% IL correspond to the fitting in the high-temperature range. Even if the FTIR results shown in Figure 1 did not show indications of the formation of γ phase in these samples after crystallization on cooling, it cannot be discarded the formation of this crystalline structure at high temperatures since crystallization in γ phase has been reported when PVDF crystallizes isothermally from the melt at the highest crystallization temperatures. The presence of multiple melting peaks on heating after isothermal crystallization seems to support the formation of multiple crystalline phases.

Thus, the crystallization kinetics is affected by the [Emim][Cl] content in the blend. Isothermal crystallization experiments were conducted in a wide range of temperatures. First, the onset of the exothermic crystallization peak in cooling scan at the rate of 90 °C/min (the maximum speed at which the DSC maintained temperature control over the entire study interval) was observed to decrease as the IL content in the mixture increases, parallel to that shown in Figure 11a for crystallization peaks. The crystallization temperature of the isothermal tests was always maintained above that onset to ensure that the crystallization process actually occurs in an isothermal manner and that the process has not been initiated before reaching the crystallization temperature.

Figure 12 shows the isothermal crystallization peaks at 140 °C in all PVDF/[Emim][Cl] blends except for the one with 40 wt% IL content. It is observed that during an initial period of time there is no growth of the crystalline fraction for PVDF/IL blends. This latency time, t_l, increases as the crystallization temperature increases (data not shown). This is a well-known phenomenon and is associated with the probability of the formation of stable nuclei which decreases the lower is the supercooling with respect to the equilibrium melting temperature [39].

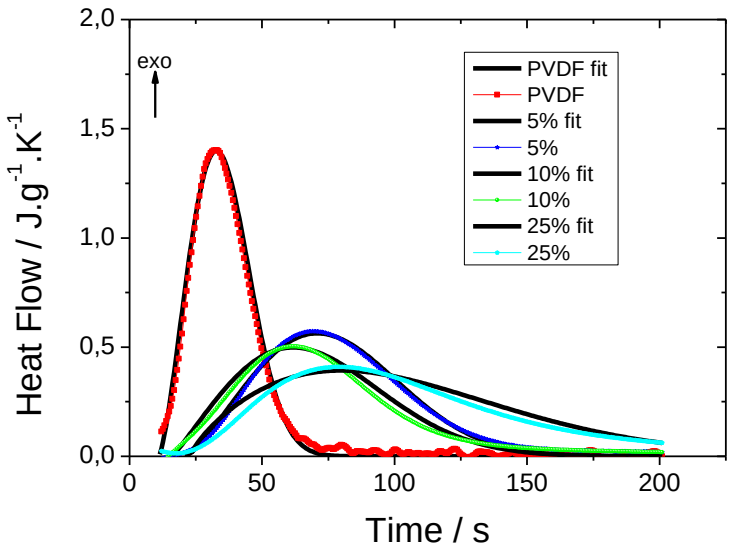

Figure 12. Isothermal crystallization peaks at 140 °C for all PVDF/IL samples except for the one with 40 wt% IL content.

It is observed that t_l does not decrease with the presence of the ionic liquid in the mixture, rather the opposite (Figure 9), which means that the ionic liquid does not favour the nucleation of the PVDF crystals. The crystallization temperature range analysed corresponds to the higher temperatures in the crystallization temperature window, and in this interval always an increase in T_c makes the kinetics slower. On the other hand, the area of the crystallization peak decreases slightly as T_c increases (data not shown).

The experimental results can be fitted with the Avrami equation [40-42]:

$$\frac{X_{ct}}{X_{c\infty}(T)} = 1 - exp(-K(t - t_l)^n) \quad (3)$$

where *n* is the Avrami's exponent related to the geometry of crystal growth, the nucleation mechanism and how the rate of incorporation of a polymer chain to growing crystal is controlled [43], and *K* is the rate constant. The fit has been usually performed by linearizing equation (3). Nevertheless, fitting of the experimental isotherms to equation (3) can be carried out by direct non-linear least squares fitting and the interval in which the results cannot be predicted by the model can be observed directly in the original diagrams [34, 44].

To do that, the heat flow delivered by the sample according to equation (3) is calculated by:

$$\dot{q}(t) = X_{c\infty}(T)\frac{\rho_c}{\rho}\Delta H_f^0 \frac{dX_c}{dt} \quad (4)$$

where $\dot{q}(t)$ is the heat flow emitted by the sample at time t, $X_{c\infty}$ is the maximum crystalline fraction at the crystallization temperature, ΔH^0_f the melting enthalpy and ρ and ρ_c are the density of the semi-crystalline PVDF and that of the crystal phase, respectively.

The crystalline mass fraction was converted to relative volumetric fraction taking into account the fully crystalline and fully amorphous polymer densities of PVDF [34]. Figure 12 shows the comparison of the experimental data of PVDF and the blends with the IL and the model equation at 140 ºC. In PVDF / IL blends with higher IL content (40 wt%), when the crystallization temperature increases, the experimental isotherm could not be reproduced by the Avrami equation.

The values of the Avrami exponent and the kinetic constant as a function of T_c for the PVDF/IL blends with different IL content are shown in Figure 13.

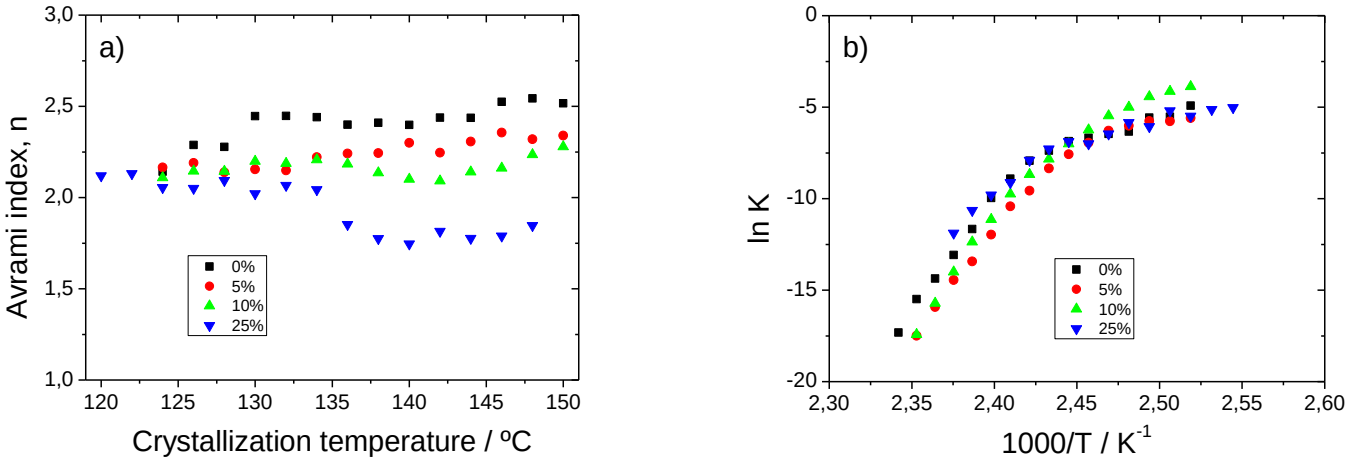

Figure 13. n (a) and K (b) parameters obtaining from adjusting the experimental results to the Avrami model.

Figure 13a) shows the evolution of the Avrami exponent, *n*, as a function of crystallization temperature showing a clear dependence on the IL content. Nevertheless, while *n* rapidly decreases when increasing the IL content at high crystallization temperatures, at low T_c it seems that the ionic liquid does not affect the crystallization kinetics so much. This feature can be related with the different behavior in the Hoffman-Weeks diagram described above.

Regarding the kinetic constant, *K*, it seems that there is a difference between the curvature of the *lnK vs 1/T* diagram of neat PVDF and that of the PVDF/IL blends (Figure 13b), being the differences more significant in the slope of the diagram at high temperatures, which can be related to the different crystalline phase which is formed in pure PVDF and in the blends.

4. DISCUSSION

Film formation from the mixture of PVDF and [Emim][Cl] in solution occurs by evaporation of the solvent at 220 °C leading to a liquid mixture of the components. Crystallization during cooling forms the PVDF crystals which grow in equilibrium with the homogeneous liquid solution. In that process, as predicted by the thermodynamics equilibrium criteria, the crystallization and subsequent melting temperatures decrease with the IL content as shown in the thermograms of Figure 8. The fact that the blends do not show a crystallization or melting peak in the temperature range of those appearing in pure PVDF demonstrates that PVDF chains separate from the liquid mixture of PVDF and the IL to incorporate to the growing crystalline lamellae.

From this assumption, during cooling, nucleation and subsequent growth of PVDF crystals occurs. FTIR spectra show that from 10 wt% up of [Emim][Cl], the ionic interaction of PVDF chains with [Emim][Cl] induces nucleation in the β-crystalline phase. Crystal growth is in the form of spherulites, as observed in the optical microscopy images of Figures 3 and 4. Crystallization in β phase is also supported by DSC

experiments. From the study of crystallization kinetics in isothermal experiments, the plot of the melting temperature against crystallization temperature (Hoffman-Weeks diagram) allows an estimation of the equilibrium melting temperature that changes sharply by passing from 10 to 25 wt% of the ionic liquid content, which supports the change of the crystalline phase formed. The crystallization kinetics itself reflects this change of behavior. The Avrami model allows a precise adjustment of the crystallization isotherms in the DSC for pure PVDF and for PVDF/IL samples with 5 and even 10 wt% IL content, but for higher IL contents the heat flow curves become very asymmetric (Figures 12 and 13) and the Avrami model stops reproducing the experimental behavior. In Figure 12 the settings up to 25% content are shown, the sample curve with 40% cannot be simulated with the model.

This again is indicative that the nucleation and growth of the PVDF crystals occurs from a liquid mixture in which the PVDF chains are homogeneously mixed with those of the [Emim][Cl], if at the initial temperature there is already separation of liquid phases one would expect a kinetics of crystallization less dependent on the composition of the mixture, although some effects would occur due to the interfacial interaction and nucleation differences if the PVDF in dispersed aggregates

In the PVDF/IL samples in which the model fitting can be performed, a clear effect of the IL content in the blends is observed, which causes the exponent of the Avrami equation to decrease. The effect on the kinetic constant, although also significant, depends on the crystallization temperature because the curvature of the representation of *lnK vs 1/T* also clearly changes with blend composition. The simultaneous formation of various crystalline phases during isothermal crystallization, in particular α and β phases in 5% and 10% samples can be observed in FTIR spectra and in the presence of more than one endotherm in the heating scans after isothermal crystallization. Nevertheless, only a peak

is observed in the isothermal DSC traces and the shape of this thermogram can be accurately reproduced with a single Avrami curve, so differences in the crystallization kinetics of the two phases cannot be distinguished by DSC.

Clear differences between the spherulites of the mixture containing 5% of IL, which crystallizes in α-phase and that which contains 25 wt% of IL, which crystallizes in β-phase, are not visible, only a smaller size of spherulite which must be interpreted as a major nucleation in the samples with 5 wt% of IL (Figure 4).

Nevertheless, during crystal growth the remaining liquid phase becomes richer in [Emim][Cl] and eventually saturates segregating at least a part of the IL. The location of the IL in the films at the end of the isothermal crystallization (the crystallization temperature of the results shown in Figures 3 to 7 was 150 ºC) has been assessed by microscopy techniques. It seems clear that although a certain content of IL remains in the spaces between the lamellae or between spherulites, a significant fraction of IL or a mixture of IL and PVDF chains in the amorphous phase is segregated towards the surface of the membrane (Note that the membrane is very thin: its thickness is in the order of magnitude of the diameters of the spherulites), as evidenced by the FESEM images of both the surface and the cross section and the EDS analysis that show the presence of chloride. The thickness of this coating cannot be measured accurately but the FESEM picture in Figure 6a allows to estimate that its thickness is below one micron and probably less than 100 nm. In any case it is worth noticing that no glass transition corresponding to pure [Emim][Cl] can be observed in the low-temperature DSC thermograms of Figure 2a. The dispersion of segregated [Emim][Cl] in very small domains and the strong interaction with PVDF segments can explain this feature. On the other hand, the glass transition of the amorphous phase of the PVDF does not progressively decrease with the increase of IL content (Figure 2), that is to say that the IL dispersed in the interlamellae

or interspherulite regions does not plasticize the amorphous phase of the PVDF what is indicative of the complex interaction between the Emim and Cl ions and PVDF chain segments.

There could still be the question of whether the phase that contains the IL after crystallization forms aggregates that cross the entire thickness of the sample, but the images of the optical microscope of Figure 4 prove that it is not so, that under a layer that contains the IL the PVDF spherulites are clearly observed.

Therefore it can be concluded that the structure of the once crystallized film consists of a continuous layer of spherulites of PVDF in the β-phase, which may contain IL in the space between spherulites or even between lamellae but some of the [Emim][Cl] is secreted forming aggregates or a thin layer on the film surface. The nanoindentation measurements clearly show the difference between the surface stiffness in the areas where the PVDF spherules appear and the deformability, with elastic modulus below the measurement threshold in the regions where the layer has formed mostly by IL (Figure 7).

5. CONCLUSION

The microstructure and crystallization kinetics of PVDF in blends with [Emim][Cl] crystallized from the melt has been studied by FESEM, OM, DSC and FTIR. PVDF crystals nucleate and grow from the liquid mixture of PVDF chains and IL molecules and the interaction with [Emim][Cl] ions induces crystallization in the β-crystalline phase, what is probed by the FTIR spectra of the blends and the changes in the crystallization kinetics. The fraction of IL in the blends is important in this sense. A 10 wt% of IL is enough to induce the formation of a 90% of β phase in the samples cooled down form the melt. Nevertheless, the DSC heating scans performed after isothermal crystallization at different temperatures show different melting peaks that could be indicative of the formation of different crystalline phases in different temperature intervals. PVDF crystal

growth segregates an amorphous phase rich in IL molecules. The ions containing chloride are detected in the core of the film although the resolution of the microscopy techniques did not allow determining in which proportion it resides in interlamellae and in the interspherulitic regions. Chloride is also detected at the surface of the film.

AUTHOR INFORMATION

Corresponding Author

cmscosta@fisica.uminho.pt (Carlos M. Costa),

Author Contributions

The manuscript was written through contributions of all authors. All authors have given approval to the final version of the manuscript

Notes

The authors declare no competing financial interest.

ACKNOWLEDGEMENTS

This work was supported by the Portuguese Foundation for Science and Technology (FCT) in the framework of the Strategic Funding UID/FIS/04650/2020. The authors thank FEDER funds through the COMPETE 2020 Programme and National Funds through FCT under the projects PTDC/BTM-MAT/28237/2017, PTDC/EMD-EMD/28159/2017 and PTDC/FIS-MAC/28157/2017. D.M.C. and C.M.C. also thank to the FCT for grants SFRH/BPD/121526/2016 and SFRH/BPD/112547/2015, respectively. Financial support from the Spanish Ministry of Economy and Competitiveness (MINECO) through the project MAT2016-76039-C4-(1 and 3)-R (AEI/FEDER, UE) (including the FEDER financial support) and from the Basque Government Industry and Education Departments under the ELKARTEK, HAZITEK and PIBA (PIBA-2018-06) programs, respectively,

are acknowledged. CIBER-BBN is an initiative funded by the VI National R&D&I Plan 2008–2011, Iniciativa Ingenio 2010, Consolider Program. CIBER Actions are financed by the Instituto de Salud Carlos III with assistance from the European Regional Development Fund.

REFERENCES

1. Drossel, W. G.; Meinel, F.; Bucht, A.; Kunze, H. Smart materials for smart production – a cross-disciplinary innovation network in the field of smart materials. *Procedia Manufacturing* **2018,** *21*, 197-204.

2. Correia, D. M.; Barbosa, C.; Costa, C. M.; Reis, P. M.; Esperanca, J. M. S. S.; Bermudez, V. D.; Lanceros-Mendez, S. Ionic Liquid Cation Size-Dependent Electromechanical Response of Ionic Liquid/Poly(vinylidene fluoride)-Based Soft Actuators. *J Phys Chem C* **2019,** *123*, 12744-12752.

3. Bauer, S.; Bauer, F. Piezoelectric Polymers and Their Applications. In *Piezoelectricity: Evolution and Future of a Technology*, Springer Berlin Heidelberg: Berlin, Heidelberg, **2008**, pp 157-177.

4. Martins, P.; Lopes, A. C.; Lanceros-Mendez, S. Electroactive phases of poly(vinylidene fluoride): Determination, processing and applications. *Prog Polym Sci* **2014,** *39*, 683-706.

5. Mejri, R.; Dias, J. C.; Hentati, S. B.; Botelho, G.; Esperanca, J. M. S. S.; Costa, C. M.; Lanceros-Mendez, S. Imidazolium-based ionic liquid type dependence of the bending response of polymer actuators. *Eur Polym J* **2016,** *85*, 445-451.

6. Correia, D. M.; Serra, R. S. I.; Tejedor, J. A. G.; Bermudez, V. D.; Balado, A. A.; Meseguer-Duenas, J. M.; Ribelles, J. L. G.; Lanceros-Mendez, S.; Costa, C. M. Ionic and conformational mobility in poly(vinylidene fluoride)/ionic liquid blends: Dielectric and electrical conductivity behavior. *Polymer* **2018,** *143*, 164-172.

7. Hu, Y. H.; Kang, W. W.; Fang, Y.; Xie, L. R.; Qiu, L. Z.; Jin, T. Piezoelectric Poly(vinylidene fluoride) (PVDF) Polymer-Based Sensor for Wrist Motion Signal Detection. *Appl Sci-Basel* **2018,** *8*, 836-848.

8. Barbosa, J. C.; Dias, J. P.; Lanceros-Mendez, S.; Costa, C. M. Recent Advances in Poly(vinylidene fluoride) and Its Copolymers for Lithium-Ion Battery Separators. *Membranes* **2018,** *8*, 45-81.

9. Liu, J. Q.; Wang, C.; Wu, X. F.; Zhu, F. F.; Liu, M.; Xi, Y. An enhanced poly(vinylidene fluoride) matrix separator with TEOS for good performance lithium-ion batteries. *J Solid State Electr* **2019,** *23*, 277-284.

10. Tandon, B.; Kamble, P.; Olsson, R. T.; Blaker, J. J.; Cartmell, S. H. Fabrication and Characterisation of Stimuli Responsive Piezoelectric PVDF and Hydroxyapatite-Filled PVDF Fibrous Membranes. *Molecules* **2019,** *24*, 1903-1923.

11. Cardoso, V. F.; Correia, D. M.; Ribeiro, C.; Fernandes, M. M.; Lanceros-Mendez, S. Fluorinated Polymers as Smart Materials for Advanced Biomedical Applications. *Polymers* **2018,** *10*, 161-187.

12. Correia, D. M.; Martins, P.; Tariq, M.; Esperanca, J.; Lanceros-Mendez, S. Low-field giant magneto-ionic response in polymer-based nanocomposites. *Nanoscale* **2018,** *10*, 15747-15754.

13. Fernandes, L. C.; Correia, D. M.; Garcia-Astrain, C.; Pereira, N.; Tariq, M.; Esperanca, J.; Lanceros-Mendez, S. Ionic-Liquid-Based Printable Materials for Thermochromic and Thermoresistive Applications. *ACS applied materials & interfaces* **2019,** *11*, 20316-20324.

14. Fernandes, L. C.; Correia, D. M.; Pereira, N.; Tubio, C. R.; Lanceros-Méndez, S. Highly Sensitive Humidity Sensor Based on Ionic Liquid–Polymer Composites. *ACS Applied Polymer Materials* **2019,** *1*, 2723-2730.

15. Ye, Y. S.; Rick, J.; Hwang, B. J. Ionic liquid polymer electrolytes. *J Mater Chem A* **2013,** *1*, 2719-2743.

16. Correia, D. M.; Costa, C. M.; Lizundia, E.; Sabater i Serra, R.; Gómez-Tejedor, J. A.; Biosca, L. T.; Meseguer-Dueñas, J. M.; Gomez Ribelles, J. L.; Lanceros-Méndez, S. Influence of Cation and Anion Type on the Formation of the Electroactive β-Phase and Thermal and Dynamic Mechanical Properties of Poly(vinylidene fluoride)/Ionic Liquids Blends. *The Journal of Physical Chemistry C* **2019,** *123*, 27917-27926.

17. Xing, C. Y.; Zhao, M. M.; Zhao, L. P.; You, J. C.; Cao, X. J.; Li, Y. J. Ionic liquid modified poly(vinylidene fluoride): crystalline structures, miscibility, and physical properties. *Polym Chem-Uk* **2013,** *4*, 5726-5734.

18. Mago, G.; Fisher, F. T.; Kalyon, D. M. Deformation-induced crystallization and associated morphology development of carbon nanotube-PVDF nanocomposites. *Journal of nanoscience and nanotechnology* **2009,** *9*, 3330-40.

19. Lopes, A. C.; Ferreira, J. C. C.; Costa, C. M.; Lanceros-Mendez, S. Crystallization kinetics of montmorillonite/poly(vinylidene fluoride) composites and its correlation with the crystalline polymer phase formation. *Thermochim Acta* **2013,** *574*, 19-25.

20. Sencadas, V.; Martins, P.; Pitaes, A.; Benelmekki, M.; Gomez Ribelles, J. L.; Lanceros-Mendez, S. Influence of ferrite nanoparticle type and content on the crystallization kinetics and electroactive phase nucleation of poly(vinylidene fluoride). *Langmuir : the ACS journal of surfaces and colloids* **2011,** *27*, 7241-9.

21. Abolhasani, M. M.; Abadchi, M. R.; Magniez, K.; Guo, Q. P. Different thermal analysis technique application in determination of fold surface-free energy. *J Therm Anal Calorim* **2015,** *119*, 527-536.

22. Xu, P.; Fu, W. J.; Cui, Z. P.; Ding, Y. S. Synergistic promotion of polar phase crystallization of PVDF by ionic liquid with PEG segment. *Appl Surf Sci* **2018,** *444*, 480-484.

23. Bahader, A.; Gui, H. G.; Nawaz, M.; Bangesh, M.; Bangesh, F.; Ibrar, M.; Ding, Y. S. Impact of ionic liquid's self-assembly on the crystallization behavior of poly (vinylidene fluoride). *J Mol Liq* **2019,** *276*, 115-119.

24. Roy, A.; Dutta, B.; Bhattacharya, S. Electroactive phase nucleation and non-isothermal crystallization kinetics study in [DEMM][TFSI] ionic liquid incorporated P(VDF-HFP) co-polymer membranes. *J Mater Sci* **2016,** *51*, 7814-7830.

25. Zhang, H.; Shi, W. H.; Cheng, H. D.; Chen, S. J.; Wang, L. M. Effect of ionic liquid on crystallization kinetics and crystal form transition of poly(vinylidene fluoride) blends. *J Therm Anal Calorim* **2018,** *132*, 1153-1165.

26. Ribeiro, C.; Costa, C. M.; Correia, D. M.; Nunes-Pereira, J.; Oliveira, J.; Martins, P.; Gonçalves, R.; Cardoso, V. F.; Lanceros-Méndez, S. Electroactive poly(vinylidene fluoride)-based structures for advanced applications. *Nature Protocols* **2018,** *13*, 681-704.

27. Efimova, A.; Pfützner, L.; Schmidt, P. Thermal stability and decomposition mechanism of 1-ethyl-3-methylimidazolium halides. *Thermochim Acta* **2015,** *604*, 129-136.

28. Cai, X.; Lei, T.; Sun, D.; Lin, L. A critical analysis of the α, β and γ phases in poly(vinylidene fluoride) using FTIR. *RSC Advances* **2017,** *7*, 15382-15389.

29. Dharaskar, S. A.; Varma, M. N.; Shende, D. Z.; Yoo, C. K.; Wasewar, K. L. Synthesis, characterization and application of 1-butyl-3 methylimidazolium chloride as

green material for extractive desulfurization of liquid fuel. *TheScientificWorldJournal* **2013,** *2013*, 395274.

30. Martins, P.; Costa, C. M.; Benelmekki, M.; Botelho, G.; Lanceros-Mendez, S. On the origin of the electroactive poly(vinylidene fluoride) β-phase nucleation by ferrite nanoparticles via surface electrostatic interactions. *CrystEngComm* **2012,** *14*, 2807.

31. Dias, J. C.; Martins, M. S.; Ribeiro, S.; Silva, M. M.; Esperança, J. M. S. S.; Ribeiro, C.; Botelho, G.; Costa, C. M.; Lanceros-Mendez, S. Electromechanical actuators based on poly(vinylidene fluoride) with [N1 1 1 2(OH)][NTf2] and [C2mim] [C2SO4]. *J Mater Sci* **2016,** *51*, 9490-9503.

32. Atkins, P.; de Paula, J. *Atkins' Physical Chemistry*. OUP Oxford: **2010**.

33. Gregorio Jr., R. Determination of the α, β, and γ crystalline phases of poly(vinylidene fluoride) films prepared at different conditions. *Journal of Applied Polymer Science* **2006,** *100*, 3272-3279.

34. Sencadas, V.; Costa, C. M.; Gómez Ribelles, J. L.; Lanceros-Mendez, S. Isothermal crystallization kinetics of poly(vinylidene fluoride) in the α-phase in the scope of the Avrami equation. *J Mater Sci* **2009,** *45*, 1328-1335.

35. Mancarella, C.; Martuscelli, E. Crystallization Kinetics of Poly(Vinylidene Fluoride). *Polymer* **1977,** *18*, 1240-1242.

36. Ducharme, S.; Bune, A. V.; Blinov, L. M.; Fridkin, V. M.; Palto, S. P.; Sorokin, A. V.; Yudin, S. G. Critical point in ferroelectric Langmuir-Blodgett polymer films. *Phys Rev B* **1998,** *57*, 25-28.

37. Hoffman, J. D.; Weeks, J. J. Melting process and the equilibrium melting temperature of polychlorotrifluoroethylene. *J. Res. Natl. Bur. Stand., Sect. A* **1962,** *66*, 13-28.

38. Sajkiewicz, P. Crystallization behaviour of poly(vinylidene fluoride). *Eur Polym J* **1999,** *35*, 1581-1590.

39. Flory, P. J.; Yoon, D. Y. Molecular morphology in semicrystalline polymers. *Nature* **1978,** *272*, 226-229.

40. Avrami, M. Granulation, Phase Change, and Microstructure - Kinetics of Phase Change. III. *J Chem Phys* **1941,** *9*, 177-184.

41. Avrami, M. Kinetics of phase change I - General theory. *J Chem Phys* **1939,** *7*, 1103-1112.

42. Avrami, M. Kinetics of Phase Change. II Transformation-Time Relations for Random Distribution of Nuclei. *The Journal of Chemical Physics* **1940,** *8*, 212-224.

43. Lorenzo, A. T.; Arnal, M. L.; Albuerne, J.; Muller, A. J. DSC isothermal polymer crystallization kinetics measurements and the use of the Avrami equation to fit the data: Guidelines to avoid common problems. *Polym Test* **2007,** *26*, 222-231.

44. Tamaño-Machiavello, M. N.; Costa, C. M.; Romero-Colomer, F. J.; María Meseguer Dueñas, J.; Lanceros-Mendez, S.; Luis Gómez Ribelles, J. Crystallization kinetics of poly(ethylene oxide) confined in semicrystalline poly(vinylidene) fluoride. *Journal of Polymer Science Part B: Polymer Physics* **2018,** *56*, 588-597.

TOC graphic

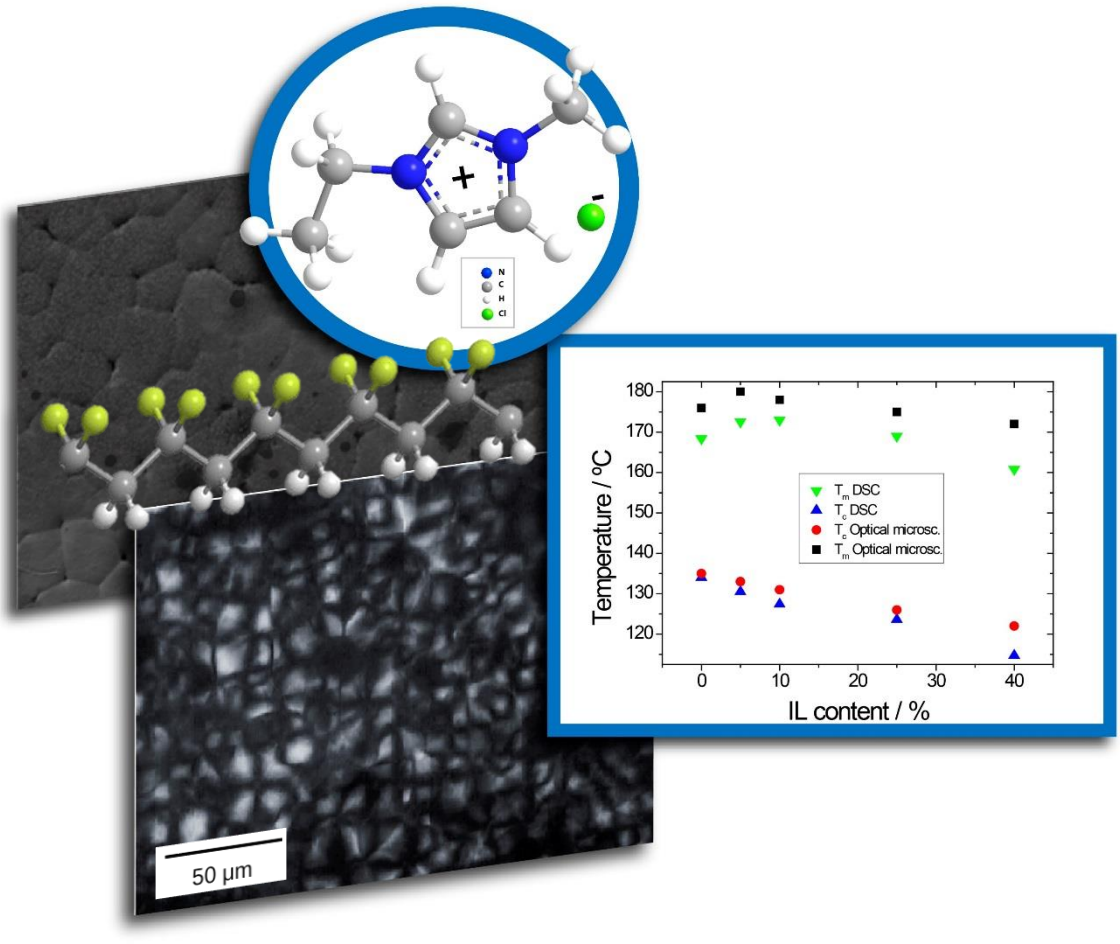

The crystallization kinetics of PVDF with IL (ionic liquid 1-ethyl-3-methylimidazolium chloride [Emim][Cl]) has been studied in which that [Emim][Cl] induces nucleation of PVDF in the electroactive and highly polar β-crystalline phase while pure PVDF crystallizes in the α phase with the same thermal treatments. The PVDF crystal growth segregates an amorphous phase rich in IL molecules on the surface of the films.